Thermodynamic properties of PbTe, PbSe, and PbS: First-principles study

Yi Zhang,[1] Xuezhi Ke,[2,1] Changfeng Chen,[1] J. Yang,[3] and P. R. C. Kent[4]

[1]*Department of Physics and High Pressure Science and Engineering Center, University of Nevada, Las Vegas, Nevada 89154, USA*
[2]*Department of Physics, East China Normal University, Shanghai 200062, China*
[3]*Materials and Processes Laboratory, GM R&D Center, Warren, Michigan 48090, USA*
[4]*Center for Nanophase Materials Sciences, Oak Ridge National Laboratory, Oak Ridge, Tennessee 37831, USA*

The recent discoveries of novel nanocomposite and doped lead chalcogenide-based thermoelectric materials have attracted great interest. These materials exhibit low thermal conductivity which is closely related to their lattice dynamics and thermodynamic properties. In this paper, we report a systematic study of electronic structures and lattice dynamics of the lead chalcogenides PbX (X=Te, Se, and S) using first-principles density-functional-theory calculations and a direct force-constant method. We calculate the structural parameters, elastic moduli, electronic band structures, dielectric constants, and Born effective charges. Moreover, we determine phonon dispersions, phonon density of states, and phonon softening modes in these materials. Based on the results of these calculations, we further employ quasiharmonic approximation to calculate the heat capacity, internal energy, and vibrational entropy. The obtained results are in good agreement with experimental data. Lattice thermal conductivities are evaluated in terms of the Grüneisen parameters. The mode Grüneisen parameters are calculated to explain the anharmonicity in these materials. The effect of the spin-orbit interaction is found to be negligible in determining the thermodynamic properties of PbTe, PbSe, and PbS.

I. INTRODUCTION

Lead chalcogenides PbTe, PbSe, and PbS have been extensively studied by experiments over the past several decades due to their potential applications as thermoelectric energy converters and electronic devices.[1] They have also attracted great theoretical interest aimed at understanding the physics of their phase transitions, electronic band gaps, and ferroelectriclike behavior at low temperatures. As narrow-gap semiconducting IV–VI compounds, lead chalcogenides exhibit outstanding optical and electrical transport properties. Meanwhile, they exhibit low thermal conductivities at high temperatures, which is unusual for simple structured materials. These unique features in electron and heat transport have made them practical thermoelectric materials for a long time.[2]

Thermoelectric materials have a large variety of applications in heating and cooling and power generation with many attractive features, such as no noise and vibration, no harmful emission, and high reliability. The parameter that determines the thermoelectric efficiency is the figure of merit defined as $ZT=\sigma S^2 T/(\kappa_L+\kappa_{elec})$, where T, S, σ, κ_L, and κ_{elec} are the absolute temperature, Seebeck coefficient, electrical conductivity, lattice thermal conductivity, and electronic thermal conductivity, respectively.[3] To increase ZT, one can either increase the power factor (σS^2) by changing the carrier concentration with doping or by using the quantum size effects;[4–6] or reduce the lattice thermal conductivity κ_L by using materials with excellent phonon-scattering ability such as skutterudites,[7,8] clathrates,[9] and thin-film superlattices.[10,11] Recently, it was reported by Hsu *et al.*[12] that *n*-type AgPb$_m$SbTe$_{2+m}$ (LAST-*m*) composites have excellent thermoelectric performance and, in particular, the *m*=18 compound has $ZT\approx2.2$ at 800 K, which is much larger than $ZT\approx0.8$ for *n*-type PbTe or $ZT=1.16$ for Sb$_2$Te$_3$ alloyed

PbTe system. Poudeu *et al.*[13] prepared a series of Pb$_{9.6}$Sb$_{0.2}$Te$_{10-x}$Se$_x$ compounds in which the phonons are strongly scattered by the nanocrystallized Se. A rather low κ_L and maximum figure of merit of $ZT\approx1.2$ was achieved at 650 K. Androulakis *et al.*[14] reported the nanostructured (PbTe)$_{1-x}$(PbS)$_x$ and (Pb$_{0.95}$Sn$_{0.05}$Te)$_{1-x}$(PbS)$_x$ have high electron mobilities and very low lattice thermal conductivities. The maximum ZT value was as high as 1.50 at 642 K. Moreover, it has been found that the introduction of thallium impurity levels in PbTe can result in a doubling of ZT to 1.5.[15] These studies suggest that the Pb chalcogenide-based materials are promising candidates for thermoelectric power generation applications.

Many *ab initio* calculations[16–21] have been performed to study the structural and electronic properties of PbTe, PbSe, and PbS. Most of the works were focused on electronic band structures and electron-transport properties. Very recently, some theoretical studies on lattice dynamics and thermodynamic functions have been reported.[22–24] The purpose of this paper is to understand the lattice dynamics of lead chalcogenides and the physical origin of their unusually low κ_L. For PbTe, PbSe, and PbS, the phonon properties such as phonon dispersion and phonon density of states (DOS) are calculated by a direct force-constant method. The electronic-structure calculations are performed to derive the necessary parameters and the effect of spin-orbit interaction (SOI) is examined. The phonon softening processes due to the volume change are carefully checked and discussed. The quasiharmonic approximation (QHA) is employed to obtain the thermodynamic functions including heat capacity, vibrational entropy, internal energy, and free energy. These calculated thermodynamic functions are in good agreement with the experimental data. Finally, the lattice thermal conductivity is evaluated in terms of the Grüneisen parameter. The mode Grüneisen parameters are calculated to illustrate the anharmonicity of different vibrational modes.

II. THEORETICAL METHODS

We carry out first-principles calculations using the local-density approximation (LDA) (Refs. 25 and 26) or generalized gradient approximation (GGA) by Perdew and Wang (Ref. 27) as implemented in the Vienna *ab initio* simulation package (VASP).[28] The projector augmented wave[29] pseudopotential method is used with a plane-wave basis set limited by the cutoff energy of 400 eV. For the primitive cell (2 atoms) and supercell (216 atoms), $16 \times 16 \times 16$ and $4 \times 4 \times 4$ Monkhorst-Pack[30] k-point grids are used, respectively. The total-energy convergences within 0.2 meV per atom are achieved when comparing the results with those using $18 \times 18 \times 18$ and $6 \times 6 \times 6$ k points for the primitive cell and the supercell, respectively. The electronic steps are carried out with the energy convergence on the order of 10^{-6} eV. The force convergence of ionic steps is set to be 10^{-5} eV/Å. The SOI is found to change the lattice constant by $\sim 0.1\%$ in these materials. So we do not include the effects of SOI except where noted.

The phonon dispersions and phonon DOS are calculated using the direct force-constant method implemented in the PHONON software by Parlinski.[31] In this method, a specific atom is displaced to calculate the induced Hellmann-Feynman (H-F) forces on itself and its surrounding atoms. By collecting the H-F forces one can construct the dynamical matrices that lead to the phonon properties and thermodynamic functions within the framework of lattice dynamics and harmonic approximation. Because of the effects of image atoms due to the periodic boundary conditions, larger supercells are needed to make sure all calculated phonon frequencies are well converged although in some high-symmetry points the wave vectors are already size-independent "exact" vectors. It is well known that lead chalcogenides exhibit strong ionicity and long-range Coulomb interaction. As a result, use of large supercells is required for good convergence. In the present work, we employed supercells with 216 atoms for phonon calculations. The calculated phonon frequencies differ by less than 0.05% compared to those obtained using supercells with 512 atoms. The atomic displacement is chosen as 0.04 Å to obtain the H-F forces. It has been pointed out that the direct force-constant method cannot directly calculate the longitudinal optical/transversal optical (LO/TO) splitting at gamma (Γ) point for polar solids such as PbTe, PbSe, and PbS.[32] In the present work, a nonanalytical term, that is, responsible for the LO/TO splitting is added to the dynamical matrix

$$\Delta D_{ij,\alpha\beta}(\mathbf{q} \to \mathbf{0}) = \frac{4\pi e^2}{\epsilon V \sqrt{M_i M_j}} \frac{(\mathbf{q} \cdot \mathbf{Z}_i^*)_\alpha (\mathbf{q} \cdot \mathbf{Z}_j^*)_\beta}{|\mathbf{q}|^2}, \quad (1)$$

where $\mathbf{q}$ is the wave vector, ϵ is the optical macroscopic dielectric function, e is the electron charge, and V is the volume of the primitive unit cell. M_i and Z_i are the mass and Born effective charge tensor for the ith atom, respectively. The α and β are the Cartesian coordinations. The Berry phase method[33] implemented in VASP is used to calculate the Born effective charge. The atom displacement chosen to calculate the electronic polarization is 0.05 Å. The calculations for both the displaced and the undisplaced system are per-

TABLE I. Structural and elastic parameters of PbTe, PbSe, and PbS. The calculated results by LDA and GGA are compared with the experimental data. The bulk modulus B and elastic constant C_{ij} are in the unit of GPa. Note that the DFT results correspond to $T = 0$ K.

	a (Å)	B	C_{11}	C_{12}	C_{44}
PbTe					
This work (LDA):	6.382	50.3	142.8	4.8	15.8
This work (GGA):	6.556	40.4	111.0	6.7	14.4
Experiment (300 K):	6.462[a]	39.8[b]	105.3[b]	7.0[b]	13.2[b]
PbSe					
This work (LDA)	6.039	58.1	153.7	11.0	17.3
This work (GGA)	6.200	49.2	123.6	12.2	17.6
Experiment (300 K)	6.124[a]	54.1[c]	123.7[c]	19.3[c]	15.9[c]
PbS					
This work (LDA)	5.842	65.6	166.0	13.9	19.4
This work (GGA)	5.992	55.7	135.1	16.9	20.4
Experiment (300 K)	5.936[a]	62.8[c]	124.0[c]	33.0[c]	23.0[c]

[a]Reference 35.
[b]Reference 36.
[c]Reference 37.

formed along three unique reciprocal vectors to obtain the average values with a set of strings of 8-k points. The dielectric constant ϵ_∞ is calculated by the optics code developed by Furthmüller.[34]

III. RESULTS AND DISCUSSION

A. Equilibrium properties and electronic structures

We first calculate the elastic constants of bulk PbTe, PbSe, and PbS. The accuracies of elastic properties determine those of the lattice-dynamics calculations. The bulk modulus is calculated by fitting the Birch-Murnaghan equation of state. A series of positive and negative strains are applied to the equilibrium structure and all atoms in the unit cell are fully relaxed. Then the elastic constants (C_{11}, C_{12}, and C_{44}) are determined by calculating the total energy as a function of strain. The calculated structural parameters and elastic constants by LDA and GGA are listed in Table I together with the experimental data for comparison. These results are also in good agreement with previous first-principles calculations.[20,21] Data in Table I show that, in general, the elastic constants calculated by GGA are in better agreement with the experimental bulk and shear moduli [$(C_{11}-C_{12})/2$, C_{44} data measured at 300 K]. Consequently, we choose to use GGA in all the following calculations.

We also study the band structure and total electron DOS for PbTe, PbSe, and PbS as shown in Fig. 1. The SOI has been considered and the results are compared to those of non-SOI calculations. In Fig. 1, it is clear that the degenerate states at high-symmetry points split after the inclusion of SOI. This is a typical relativistic effect of the *s-p* splitting as pointed out by Rabe.[17] The non-SOI direct band gap of PbTe
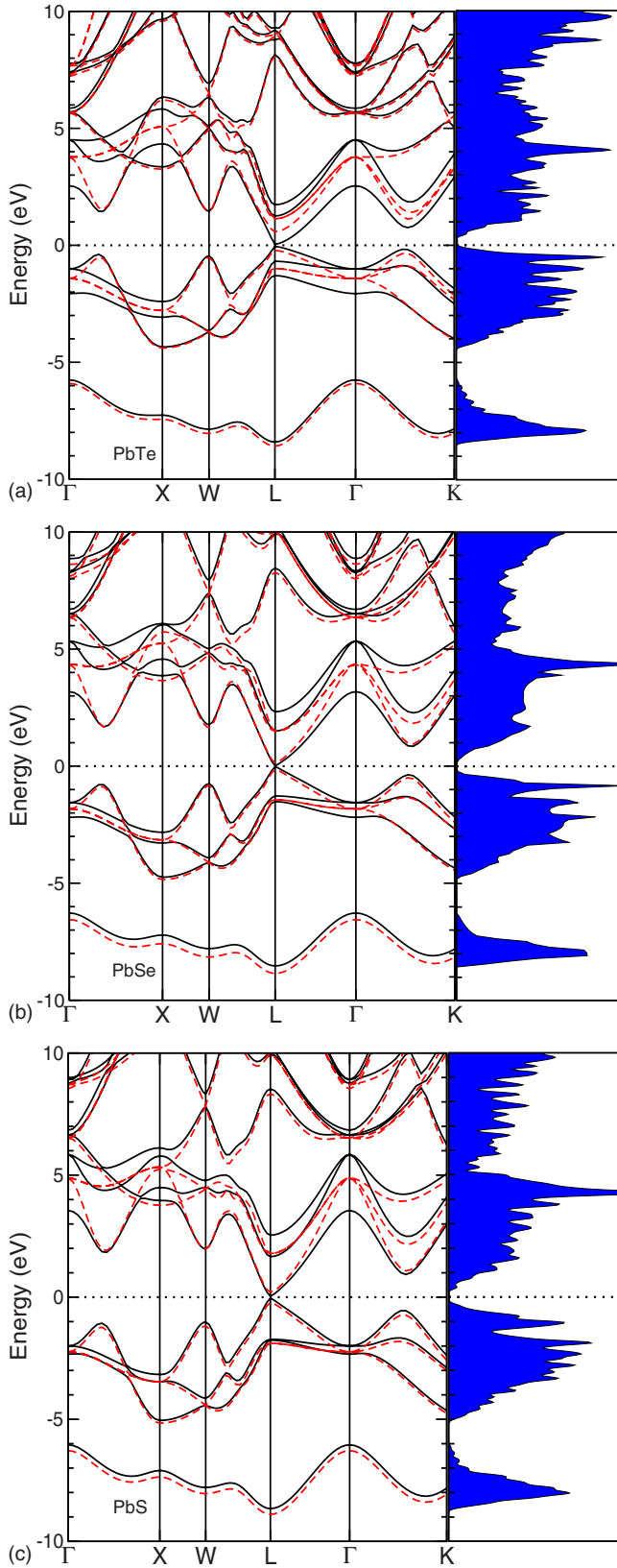
FIG. 1. (Color online) Electronic band structure and total electron DOS for (a) PbTe, (b) PbSe, and (c) PbS. The solid (in black) and dash lines (in red) are the band structures with and without SOI, respectively. The total electron DOS (normalized) in the right panels are results with SOI. The zero energy is set to be Fermi level.

TABLE II. The calculated and experimental energy gaps (in eV) at L and Γ points for PbTe, PbSe, and PbS. Both the SOI and the non-SOI results are presented.

		SOI	Non-SOI	Experiment[a]
PbTe:	$E_g(L)$	0.091	0.806	0.19
	$E_g(\Gamma)$	3.554	5.195	
PbSe:	$E_g(L)$	0.022	0.310	0.17
	$E_g(\Gamma)$	4.733	6.173	
PbS:	$E_g(L)$	0.074	0.440	0.29
	$E_g(\Gamma)$	5.545	7.124	

[a]Reference 37.

at L point is 0.806 eV, which is larger than the 0.645 eV calculated in a previous work.[20] For SOI calculations, the same band gap is reduced to 0.091 eV, which is smaller than the experimental value 0.19 eV (see Table II). For PbSe and PbS, the SOI band gap at L point are 0.022 and 0.074 eV, respectively, indicating these two materials are also narrow band-gap semiconductors. However, the calculated band gaps are much smaller than the corresponding experimental values of 0.17 and 0.29 eV.[37] The band structures for PbTe, PbSe, and PbS are similar in shape along the high-symmetry lines in Fig. 1 with some slight differences in energy levels at Γ and L points. This is also in good agreement with previous work.[20]

B. Born effective charge, phonon dispersion, and phonon density of states

The calculated dielectric constants and Born effective charges are listed in Table III. Because all three materials possess the rock salt structure, the off-diagonal elements of the Born effective charge tensor are all zero and the three diagonal elements Z_{xx}, Z_{yy}, and Z_{zz} are the same for each material. Moreover, the binary compounds in the form of "AB" have the relation $Z_A^* = -Z_B^*$. Therefore, only $Z_{Pb,xx}^*$ (Z^*) is calculated here. The dielectric constant ϵ_∞ is calculated with the optics code developed by Furthmüller.[34] It is common for III–V compounds that LDA and GGA underestimates the energy band gaps. Accurate band gaps are crucial in determining the dielectric constants. As a result, the cal-

TABLE III. Calculated and measured dielectric constant ϵ_∞ and Born effective charge Z^* (in e). The experimental Born effective charges are derived from the experimentally measured LO/TO splittings.

		This work	Experiment[a]
PbTe:	ϵ_∞	25.26	32.8
	Z^*	5.80	6.5
PbSe:	ϵ_∞	19.23	22.9
	Z^*	4.89	4.9
PbS:	ϵ_∞	16.42	17.2
	Z^*	4.48	4.4

[a]Reference 38.

culated dielectric constants for PbTe, PbSe, and PbS are 23.0%, 16.0%, and 4.5% smaller than their experimental counterparts, respectively. Better results are expected by applying band-gap corrections such as the GW methods. Z^* cannot be measured directly. Instead, we derived Z^* by comparing the measured LO/TO splittings to our first-principles results. Interestingly, a combination of effective charge and dielectric constant from either theory or experiment leads to similar LO/TO splitting values at Γ point. The calculated Z^* is much larger than the +2 nominal charge for Pb (-2 for Te, Se, and S) in the Pb chalcogenides, indicating that LO/TO splittings at the Γ points for these materials are significant. On the other hand, large Z^* suggests that the Pb chalcogenides can be strongly polarized with distortions or atomic displacements.

Recently, it has been pointed out that the SOI effect could be important for studying thermodynamic properties of heavy element materials such as bismuth (Bi).[39] Therefore, we also performed test calculations on Bi. It was found that the DFT-optimized lattice parameter for Bi with SOI is 0.93% larger than that without SOI. This is much larger than the ~0.1% lattice-parameter difference for PbTe, PbSe, and PbS. From the viewpoint of electronic band structure, this could be due to the larger SOI energy level splittings for Bi. On the other hand, a study of Sb showed[40] only slight improvement in the calculated specific-heat values with SOI. The calculated lattice parameters for Sb with and without SOI differ only by 0.1%. In our studies, the SOI DFT-optimized lattice parameters of PbTe, PbSe, and PbS are 6.558, 6.191, and 5.985 Å, respectively, which are only ~0.1% smaller than the non-SOI results. As a result, we decided not to include SOI in our phonon calculations since the SOI effect is small and the related calculations are very time consuming.

The calculated phonon-dispersion relations for PbTe, PbSe, and PbS are shown in Fig. 2. The calculated phonon frequencies at high-symmetry points are listed in Table IV. Remarkable splittings occur between T_{1u}(LO) and T_{1u}(TO) at Γ point. This is an expected result since the calculated Born effective charges are unusually large. An interesting feature for these compounds, as has been pointed out by many previous work,[17,35] is that the TO modes are very soft and their frequencies decrease with decreasing temperature near the Brillouin-zone center. In our study, the TO frequency at Γ point is 1.04, 1.26, and 1.91 THz for PbTe, PbSe, and PbS, respectively, which is in good agreement with the available experimental data at 300 K (see Table IV).[41,42] This is due to the accurate calculations of elastic parameters by GGA. It should be noted that the temperature dependence of TO frequencies cannot be obtained in the present work. This is because the soft TO modes near the zone center are stabilized by the temperature-dependent anharmonic interactions through phonon renormalization processes,[17] which are difficult to describe quantitatively by first-principles calculations. PbS has higher optic-phonon branches in frequency than PbTe and PbSe. This is because Pb and S have the largest atomic mass disparity. As a result, the overlap between longitudinal acoustic (LA) and TO branches along the plotted lines, which is obvious for PbTe and PbSe, does not occur for PbS. However, one should ex-
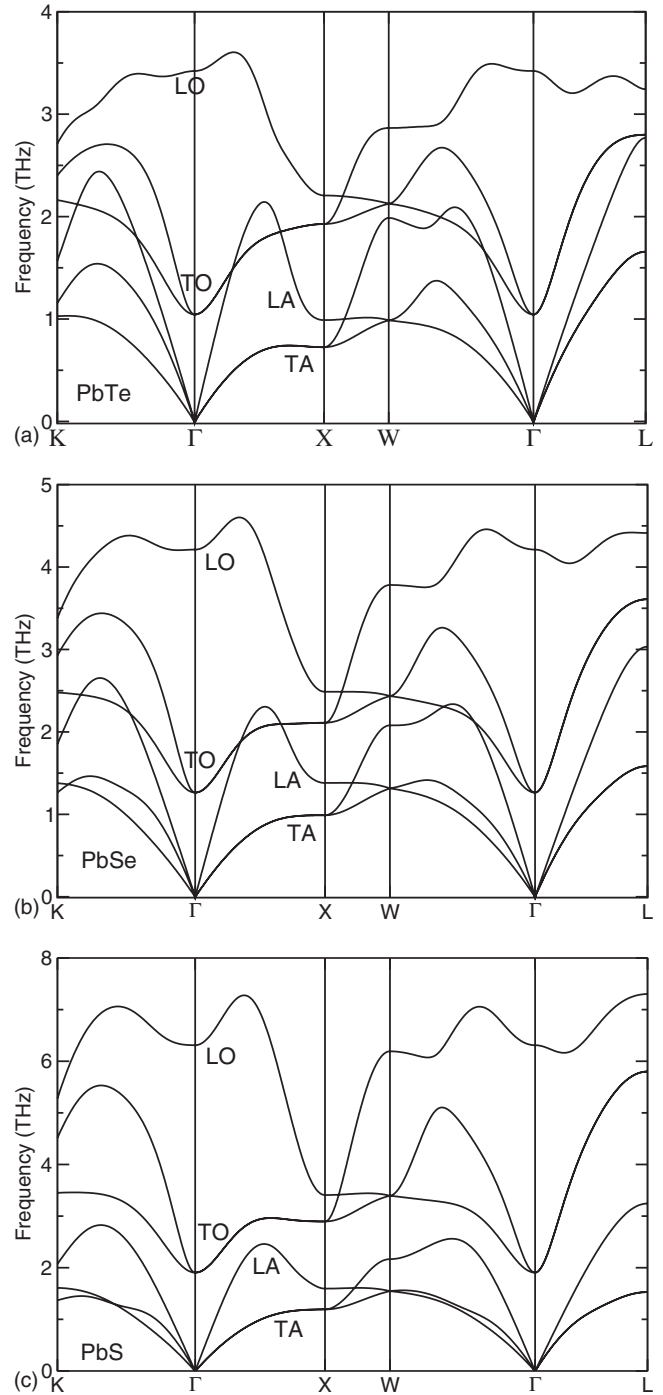
FIG. 2. Calculated phonon dispersions of PbTe, PbSe, and PbS. The phonons were calculated by using equilibrium volume.

pect strong LA-TO interaction in all three materials according to the phonon dispersions. The visible dispersions of TO branches for all samples show that Pb and Te (Se, S) atoms are somewhat coupled, indicating that the Pb-Te (Se, S) bonds are partially covalent. This is in contrast to NaCl whose TO dispersions are much flatter.[43]

The total and projected phonon DOS for PbTe, PbSe, and PbS are plotted in Figs. 3(a)–3(c), respectively. One can observe a sharp low-frequency peak mainly contributed by Pb for these materials. PbTe has a second low-frequency peak

TABLE IV. Calculated and measured phonon frequencies in THz for PbTe and PbS at high-symmetry points. The two transverse modes (TA and TO) are degenerate at these points. The experimental data for PbSe is not available in the literature.

PbTe		LA	TA	LO	TO
(0,0,0)	Calc.:	0	0	3.42	1.04
	Expt.:[a]	0	0	3.42	0.95
(0.5,0,0)	Calc.:	0.73	0.99	2.21	1.93
	Expt.:[a]	0.72	0.98	2.35	2.08
(0.5,0.5,0.5)	Calc.:	2.79	1.66	3.24	2.80
	Expt.:[a]	2.74	1.63	2.86	2.72
PbSe		LA	TA	LO	TO
(0,0,0)	Calc.:	0	0	4.29	1.43
(0.5,0,0)	Calc.:	1.43	1.01	2.58	2.23
(0.5,0.5,0.5)	Calc.:	3.07	1.63	4.47	3.68
PbS		LA	TA	LO	TO
(0,0,0)	Calc.:	0	0	6.31	1.91
	Expt.:[b]	0	0	6.70	1.95
(0.5,0,0)	Calc.:	1.60	1.19	3.41	2.90
	Expt.:[b]	1.64	1.20	2.77	2.65
(0.5,0.5,0.5)	Calc.:	3.24	1.53	7.30	5.80
	Expt.:[b]	3.05	1.48	7.13	5.82

[a]Reference 41.
[b]Reference 42.

located at 1.5 THz that does not exist for PbSe or PbS. It is clear that the projected phonon DOS of Pb and X ($X=$Te, Se, and S) dominate the low and high-frequency domain, respectively. This is due to the atomic mass difference that results in the separation of acoustic- and optic-phonon branches. For PbTe, a slight overlap between the projected phonon DOS of Pb and Te near 1.0 THz can be found, which is not clearly seen for PbSe (Pb and Se) or PbS (Pb and S).

Next we present phonon calculations using a variety of lattice parameters to study phonon stability and softening modes for PbTe, PbSe, and PbS. Figure 4 plots phonon dispersions of PbTe at two critical points beyond which the softened phonon vibration modes become unstable. In Fig. 4(a), the transverse-acoustic (TA) phonon branches become soft in the $\Gamma \rightarrow X$ (1/2, 1/2, 0), $\Gamma \rightarrow W$ (3/4, 1/2, 1/4) and $\Gamma \rightarrow K$ (3/8, 3/4, 3/8) directions with increasing pressure. This is consistent with the previous observations of PbTe under pressure.[44] The corresponding lattice parameter and pressure are 6.10 Å and 14.3 GPa, respectively. The critical pressure is much larger than the 6 GPa for the first [$B1$("NaCl") $\rightarrow Pnma$] phase transition[45] but comparable to the 13 GPa needed for the second [$Pnma \rightarrow B2$("CsCl")] transition.[46] Therefore, the first phase transition ($B1 \rightarrow Pnma$) could not be induced by the TA phonon instability. The soft TO modes are also found to be very sensitive to the volume change. Figure 4(b) shows a pronounced drop in the TO frequency to 0.61 THz near the zone center with only 0.76% increase in

lattice parameter. The strong volume dependence of soft TO and TA modes suggests that there might be significant anharmonicity in PbTe.

The critical points for PbSe are determined and the calculated phonon dispersions are plotted in Fig. 5. In Fig. 5(a), the TA phonon branches in the $\Gamma \rightarrow X$ direction become soft with increasing pressure. But the phonon branches in the $\Gamma \rightarrow W$ and $\Gamma \rightarrow K$ directions remain unchanged with linear dispersion relations. Further compression will result in the breakdown of TA modes along all three directions. The corresponding lattice parameter and pressure are 5.70 Å and 21.8 GPa, respectively. This critical pressure is larger than the 4.5 GPa for the first phase transition [$B1 \rightarrow B16$("GeS")]. The TO softening at Γ point in Fig. 5(b) is quite similar to that of PbTe. The TO modes drop to 0.73 THz when the lattice parameter and pressure are 6.25 Å and -1.1 GPa, respectively. The phonon dispersions for PbS at critical points are plotted in Fig. 6. In Fig. 6(a), the soft TA phonon branches behave almost the same as those in PbSe under compression. The corresponding critical lattice parameter and pressure are 5.50 Å and 25.0 GPa, respectively. The pressure is larger than the 2.2 GPa for phase transition of $B1 \rightarrow B16$. Again, the TO modes become soft at Γ point with the unit cell expanded. From the discussion above, one can conclude that PbSe and PbS are similar in terms of the phonon stability behavior. PbTe, on the other hand, behaves differently. This could be responsible for the different intermediate phases for PbTe ($Pnma$) and PbSe ($B16$"GeS") under pressure.[46]

C. Thermodynamic functions

With the calculated phonon DOS, we are able to determine various thermodynamic functions. The heat capacity at the constant volume C_v is given by

$$C_v = rk_B \int_0^\infty d\omega g(\omega) \left(\frac{\hbar\omega}{k_BT}\right)^2 \frac{\exp\left(\frac{\hbar\omega}{k_BT}\right)}{\left[\exp\left(\frac{\hbar\omega}{k_BT}\right)-1\right]^2}, \quad (2)$$

where $g(\omega)$ is the phonon DOS of the unit cell, r is the number of degrees of freedom in the unit cell, $\hbar$ is the Planck constant, k_B is the Boltzmann constant, and ω is the phonon frequency. The limits of C_v at 0 K and high temperature are 0 and rk_B, respectively. In the quasiharmonic approximation, the relation between C_v and C_p (heat capacity at constant pressure) is

$$C_p - C_v = \alpha^2(T)BVT, \quad (3)$$

where α is the thermal-expansion coefficient of volume defined as $(1/V)(\partial V/\partial T)$, B is the bulk modulus, and V is the volume of the system. The vibrational entropy at a finite temperature is defined by
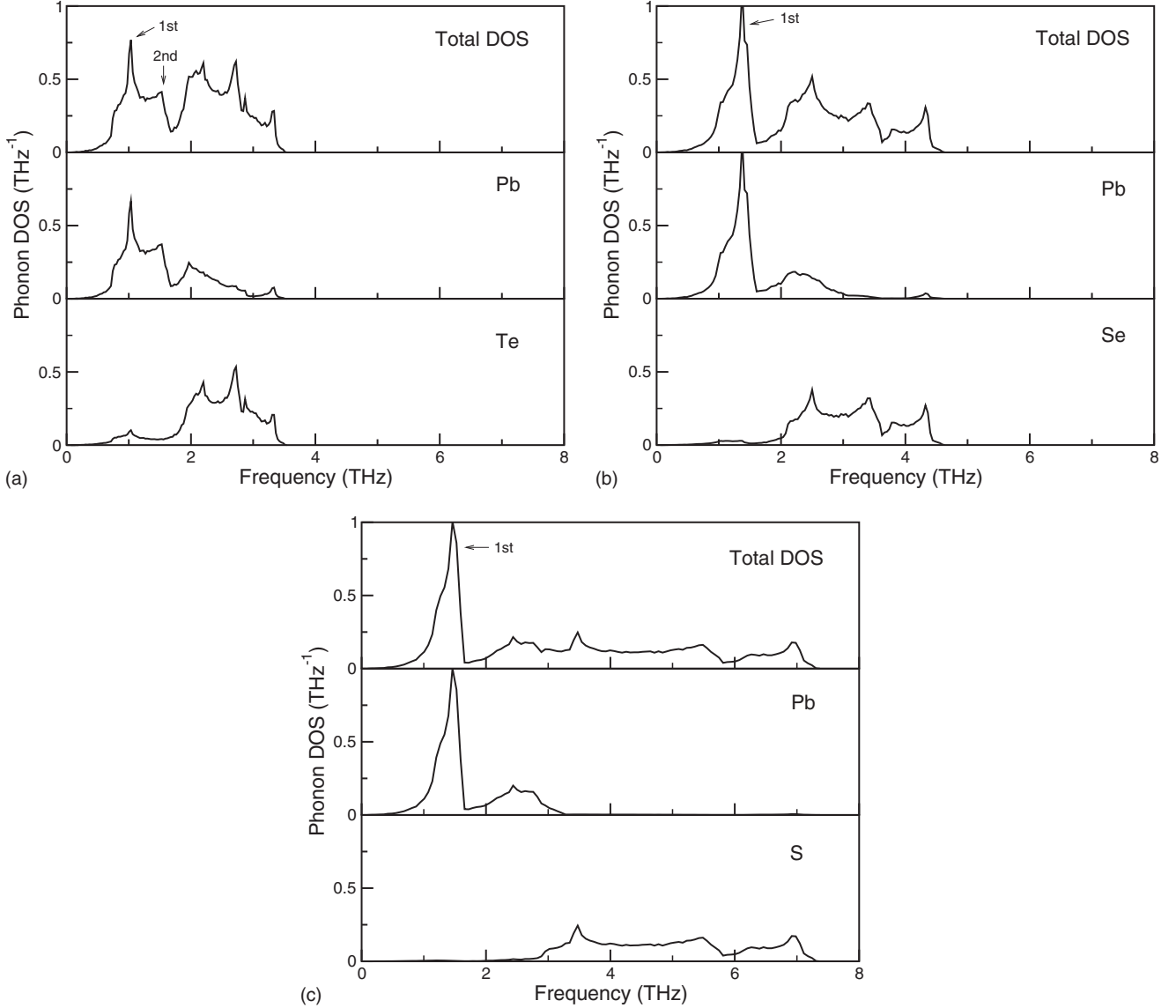
FIG. 3. Calculated total and projected phonon density of states for (a) PbTe, (b) PbSe, and (c) PbS.

$$S(T) = rk_B \int_0^\infty g(\omega) \left\{ \left(\frac{\hbar\omega}{2k_BT} \right) \left[\coth\left(\frac{\hbar\omega}{2k_BT} \right) - 1 \right] \right.$$
$$\left. - \ln\left[1 - \exp\left(\frac{-\hbar\omega}{k_BT} \right) \right] \right\} d\omega. \qquad (4)$$

The internal energy of the unit cell is calculated by

$$U(T) = \frac{1}{2} r \int_0^\infty \hbar\omega g(\omega) \coth\left(\frac{\hbar\omega}{2k_BT} \right) d\omega. \qquad (5)$$

By calculating the thermodynamic functions above, we can obtain the Helmholtz free energy $F(T)$ of the unit cell from the relation

$$F(T) = E_{elec} + U(T) - TS(T), \qquad (6)$$

where E_{elec} is the electronic energy of the unit cell calculated by the first-principles total-energy calculations.

In order to study the thermal-expansion effects that are related to the anharmonicity of these materials, we use the QHA, in which the phonons are considered as harmonic but volume dependent. In our calculations, the unit cells are expanded and compressed to a set of constant volumes with the cell shape and atomic positions fully relaxed. Then the equilibrium volume at temperature T is obtained by minimizing the free energy. The calculated free energy versus lattice-parameter curves for PbTe, PbSe, and PbS are plotted in Figs. 7(a)–7(c), respectively. The unit cells are expanded less than 3% because the critical points for expansion are quite close to the equilibrium states. The equilibrium lattice parameters, bulk modulus, and linear thermal expansivities $[=(1/L)(\partial L/\partial T)]$ at different temperatures are obtained by fitting the third-order Birch-Murnaghan equation of state. The calculated data are compiled in Table V. It is noted that the linear thermal expansivity is 1/3 of the volume thermal expansivity. PbTe has the largest thermal expansivity at low temperatures. It is surpassed by PbS when the temperature is
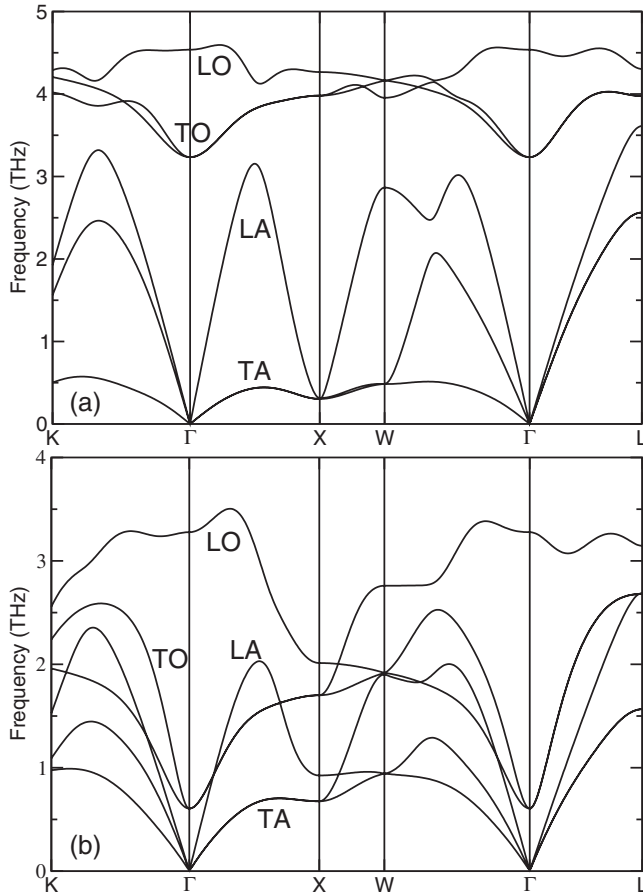
FIG. 4. Calculated phonon dispersions of PbTe at critical points. (a) Compressed PbTe with the lattice parameter of 6.10 Å at 14.3 GPa pressure. (b) Expanded PbTe with the lattice parameter of 6.60 Å at −0.8 GPa pressure.

FIG. 5. Calculated phonon dispersions of PbSe at critical points. (a) Compressed PbSe with the lattice parameter of 5.70 Å at 21.8 GPa pressure. (b) Expanded PbSe with the lattice parameter of 6.25 Å at −1.1 GPa pressure.

above 150 K. This order of thermal expansivity is in agreement with the experimental measurements.[35] In general, QHA is valid when the temperature is much lower than the melting point where the anharmonic effect is dominant.[47] For PbTe, PbSe, and PbS, the melting temperatures are around 1000 K and much higher than the maximum temperature (300 K) in our studies. However, the calculated thermal expansivity at 300 K is about 1/3 larger than the experimental data although the theory and experiment agree well below 150 K.[35] This is due to the strong anharmonicity at room temperature for these materials. Anharmonicity will grow even stronger with increasing temperature. We expect, therefore, using QHA at $T > 300$ K would lead to even larger errors.

The calculated and measured thermodynamic functions as a function of temperature for PbTe, PbSe, and PbS are shown in Fig. 8, in which the (a), (b), and (c) are C_v and C_p, internal energy of $U(T) - U(20)$, and entropy of $S(T) - S(20)$, respectively. $U(20)$ and $S(20)$ corresponds to the internal energy and entropy at 20 K, respectively. The experimental data between 20 and 260 K are taken from the work of Parkinson et al.[48] As shown in Fig. 8, the calculated thermodynamic functions are in good agreement with the experimental data. These results indicate that QHA is valid in predicting thermodynamic functions under 300 K. PbSe has nevertheless an

unusually large experimental $C_p(C_v)$ value of 35.28 J mol^{-1} K^{-1} at 25 K. We do not know the origin of this discrepancy between our calculations and the experimental data.

D. Grüneisen parameter and thermal conductivity

The lattice thermal conductivity κ_L is determined by various phonon-scattering mechanisms such as the phonon-phonon interaction and the defect scattering. At high temperatures, the Umklapp processes are dominant in scattering heat-conducting phonons. Assuming the heat is conducted only by acoustic phonons and the phonon-phonon interactions are all anharmonic Umklapp processes, the lattice thermal conductivity is given by[49]

$$\kappa_L = A \frac{\bar{M} \theta^3 \delta}{\gamma^2 n^{2/3} T}, \tag{7}$$

where $\bar{M}$ is the average atomic mass in the unit cell, θ is the Debye temperature, δ^3 is the volume per atom, and n is the number of atoms in the primitive cell. A is a physical constant $\approx 3.1 \times 10^{-6}$ if κ_L is in W/mK, $\bar{M}$ in amu, and δ in Å. γ is the high-temperature limit of the acoustic-phonon Grüneisen parameter defined as
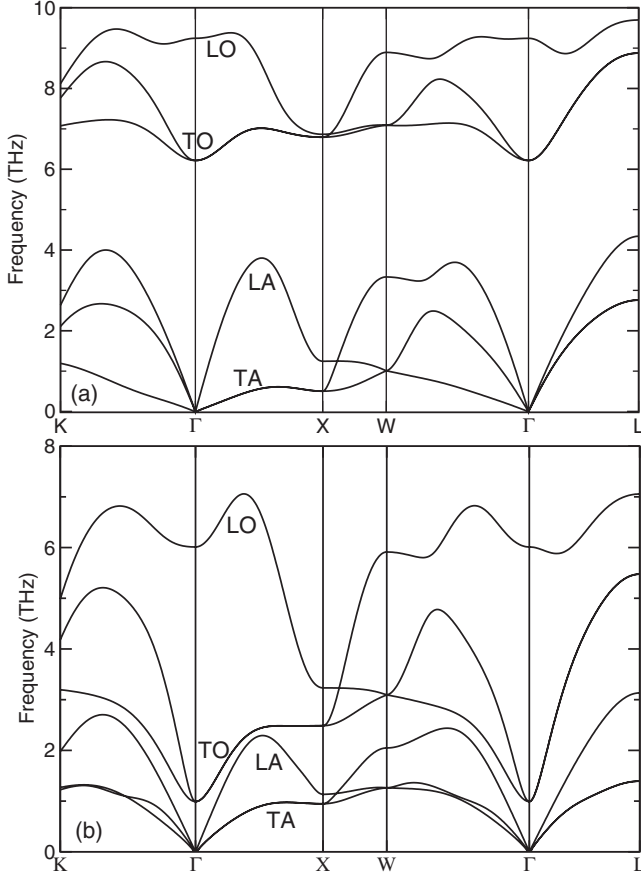
FIG. 6. Calculated phonon dispersions of PbS at critical points. (a) Compressed PbS with the lattice parameter of 5.50 Å at 25.5 GPa pressure. (b) Expanded PbS with the lattice parameter of 6.05 Å at −1.5 GPa pressure.

$$\gamma = \frac{\alpha B V_m}{C_v}, \qquad (8)$$

where V_m is the molar volume.

The values of γ for PbTe, PbSe, and PbS at 300 K are calculated by using experimental data at room temperature.[35–38,48] The obtained results are 1.96, 2.23, and 2.52, respectively. The corresponding lattice thermal conductivity values are 2.01, 1.75, and 4.14 W/mK, respectively. For PbTe and PbSe, the lattice thermal conductivity agrees well with the experimental data at 300 K (see Table [VI]).[50] κ_L is very sensitive to the Debye temperature [Eq. (7)]. For PbS, the Debye temperature is highly temperature dependent, which may result in strong deviation of phonon spectrum from the Debye model. As a result, the calculated κ_L for PbS is much larger than the experimental value of 2.5 W/mK. In addition, we calculate $\gamma = 2.18$, 2.29, and 2.50 for PbTe, PbSe, and PbS, respectively, when all the input parameters for Eq. (7) are taken from the first-principles calculations. The resulting κ_L are 1.66, 1.52, and 4.29 W/mK, respectively, which are less accurate but still in reasonable agreement with the experimental data. This is because GGA underestimates bulk modulus and overestimates lattice parameter. Moreover, as discussed in the previous section,

our theoretical calculations do not predict thermal expansivity accurately over 150 K. The calculated data, however, do show the same order $[\kappa_L^{cal2}(\mathrm{PbS}) > \kappa_L^{cal2}(\mathrm{PbTe}) > \kappa_L^{cal2}(\mathrm{PbSe})]$ as that of the experimental data.

According to Eq. (7), the calculated low lattice thermal conductivities are attributed to the large acoustic-phonon Grüneisen parameters γ that reflect the anharmoncities of acoustic-phonon modes. On the other hand, the optical phonons could be important in scattering heat conducting acoustic phonons through anharmonic phonon-phonon interactions since the TO and LA branches are close.

The average Grüneisen parameter is defined as the weighted average of mode Grüneisen parameters $\gamma_n(\mathbf{q})$

$$\gamma_{ave} = \frac{1}{C_v} \sum_{\mathbf{q},n} \gamma_n(\mathbf{q}) c_{vn}(\mathbf{q}), \qquad (9)$$

where $C_{vn}(\mathbf{q})$ is the contribution from the nth phonon branch with wave vector $\mathbf{q}$ to the total specific heat.

The mode Grüneisen parameter $\gamma_n(\mathbf{q})$ describes the phonon frequency shift with respect to the volume and is given by

$$\gamma_n(\mathbf{q}) = -\frac{d[\ln \omega_n(\mathbf{q},V)]}{d[\ln V]}, \qquad (10)$$

where $\omega_n(\mathbf{q},V)$ is the phonon frequency of the nth branch with wave vector $\mathbf{q}$. These mode Grüeisen parameters, which reflect the anharmonicity of different phonon modes, can be obtained by phonon calculations.

In order to shed some light on the anharmonic effect, we calculate the mode Grüneisen parameters of all six phonon branches for PbTe, PbSe, and PbS at different wave vectors, as plotted in Figs. 9(a)–9(c), respectively. The phonon frequency shifts are obtained by expanding and compressing the equilibrium volume by 1%. It is seen that the calculated mode Grüneisen parameters throughout the Brillouin zone are all positive, indicating that phonon frequencies increase with decreasing volume. For all three materials, peaks at Γ points correspond to very high mode Grüneisen parameters. Analyses show that these top branches in all three materials are the TO vibrational modes. This is consistent with the sensitive TO phonon shift with respect to the volume change as discussed in the previous section. For PbS, the peaks of TO branches are not as high as those of PbTe and PbSe. Nevertheless, its LA and TA phonon branches have larger mode Grüneisen parameters along the $X \rightarrow W$ and $\Gamma \rightarrow K$ directions. Consequently, PbS has the largest acoustic-phonon Grüneisen parameter γ. The calculated mode Grüneisen parameters are very large as compared to other known solids with large mode Grüneisen parameters $[\gamma_n(\mathbf{q}) < 5$ for Zn,[51] Al,[52] AlLi$_3$,[52] and Mg$_2$SiO$_4$ (Ref. [53])], which may indicate strong anharmonic interactions between optic and acoustic
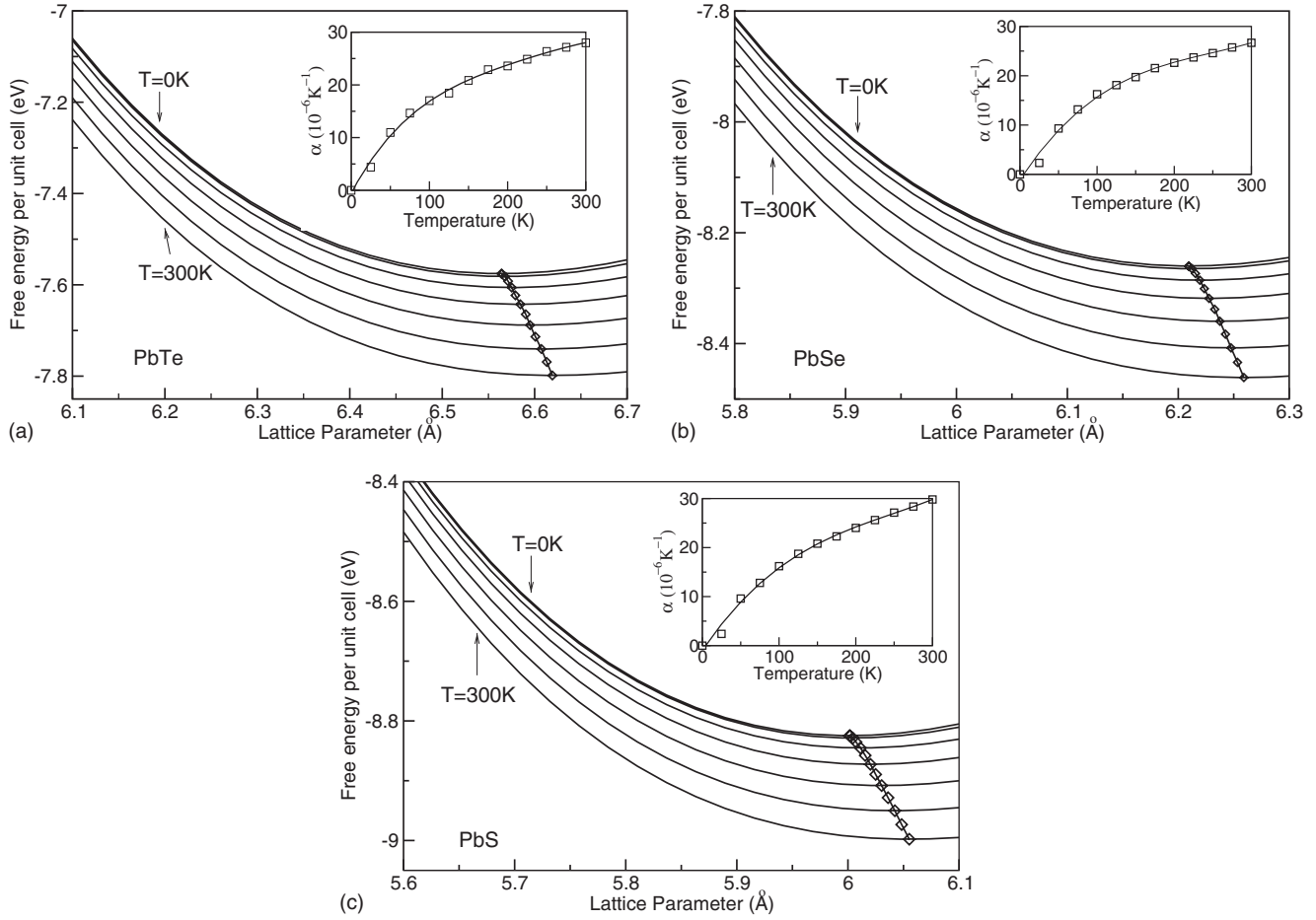
FIG. 7. Calculated Helmholtz free energy $F(T)$ as a function of lattice parameter for (a) PbTe, (b) PbSe, and (c) PbS. There are seven free-energy curves (solid lines) plotted in each figure range from 0 to 300 K with $\Delta T=50$ K. The diamond symbols represent the energy minima at different temperatures. The insets are fittings of linear thermal expansivities as a function of temperature.

phonons and an additional scattering to the heat-conducting phonons. This could be the reason for the difference between the calculated and the experimental lattice thermal conductivity of PbS. The contributions from other phonon-scattering mechanisms such as the defect scattering are neglected in this study because of the good agreement of κ_L between theory and experiment, except for PbS in which the impurity scattering could still be important.

TABLE V. Lattice parameter, bulk modulus, and linear thermal expansivity for PbTe, PbSe, and PbS from 0 to 300 K. The equilibrium lattice parameter and bulk modulus are obtained by fitting the energy curves using the Birch-Murnaghan equation of state.

	0 K	50 K	100 K	150 K	200 K	300 K
PbTe						
Lattice parameter (Å)	6.564	6.568	6.575	6.585	6.595	6.619
Bulk modulus (GPa)	39.6	38.7	37.2	35.7	34.1	30.7
Thermal expansivity (10^{-6}/K)	0	10.97	17.01	20.85	23.59	27.99
PbSe						
Lattice parameter (Å)	6.209	6.212	6.220	6.228	6.238	6.259
Bulk modulus (GPa)	48.4	47.6	46.2	44.7	43.1	39.9
Thermal expansivity (10^{-6}/K)	0	9.31	16.25	19.72	22.63	26.69
PbS						
Lattice parameter (Å)	6.002	6.004	6.011	6.020	6.030	6.055
Bulk modulus (GPa)	54.6	53.6	51.6	49.5	47.2	42.3
Thermal expansivity (10^{-6}/K)	0	9.60	16.21	20.81	24.01	29.81
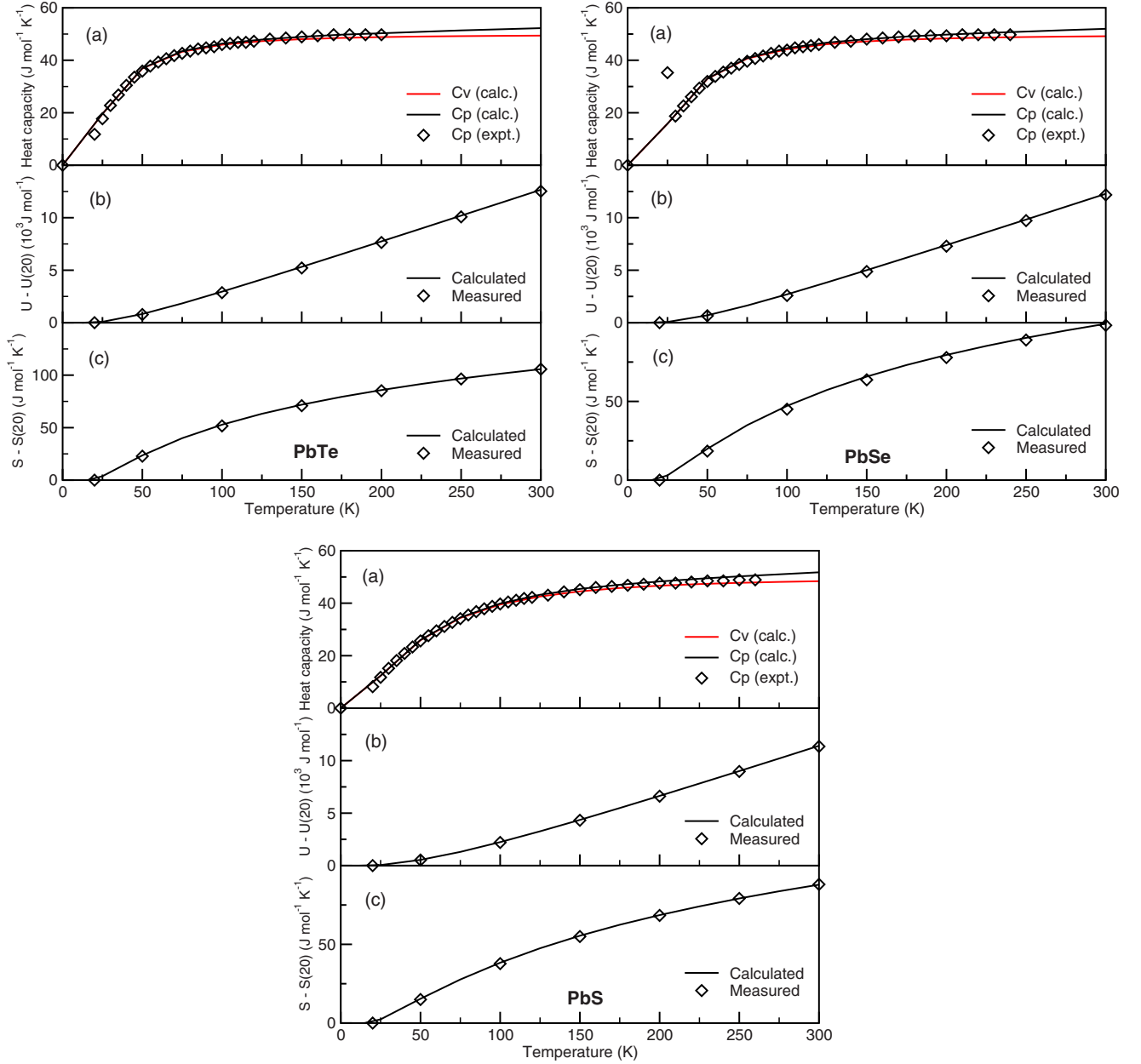
FIG. 8. (Color online) Calculated thermodynamic functions as a function of temperature for PbTe, PbSe, and PbS. The panel (a), (b), and (c) represents heat capacity, internal energy $U-U(20)$, and entropy $S-S(20)$, respectively. $U(20)$ and $S(20)$ are internal energy and entropy at 20 K, respectively. The diamond symbols are experimental data.

IV. CONCLUSIONS

We have performed first-principles density-functional-theory calculations to study the electronic- and lattice-dynamics properties of the lead chalcogenides (PbTe, PbSe, and PbS). The lattice parameters and elastic moduli are calculated using LDA and GGA and are compared to previous calculations and experimental results. The electronic band structures and DOS have been calculated with the inclusion of SOI. The results show that these three materials are narrow-gap semiconductors with similar dispersion curves. Moreover, SOI can strongly affect the size of the band gap. Our results also show that SOI causes the *s-p* splitting at high-symmetry points but has little effect in changing the DFT-optimized lattice parameters.

TABLE VI. The calculated acoustic-phonon Grüneisen parameter and lattice thermal conductivity and the experimental lattice thermal conductivity κ_L^{exp}. The physical parameters for calculating γ^{cal1} and κ_L^{cal1} are from experiment data and the parameters for γ^{cal2} and κ_L^{cal2} are from the first-principles calculations. All the thermal conductivities κ_L are in W/mK.

	γ^{cal1}	κ_L^{cal1}	γ^{cal2}	κ_L^{cal2}	$\kappa_L^{\mathrm{exp\ a}}$
PbTe	1.96	2.01	2.18	1.66	2.0
PbSe	2.23	1.75	2.29	1.52	1.6
PbS	2.52	4.14	2.50	4.29	2.5

[a]Reference 50.
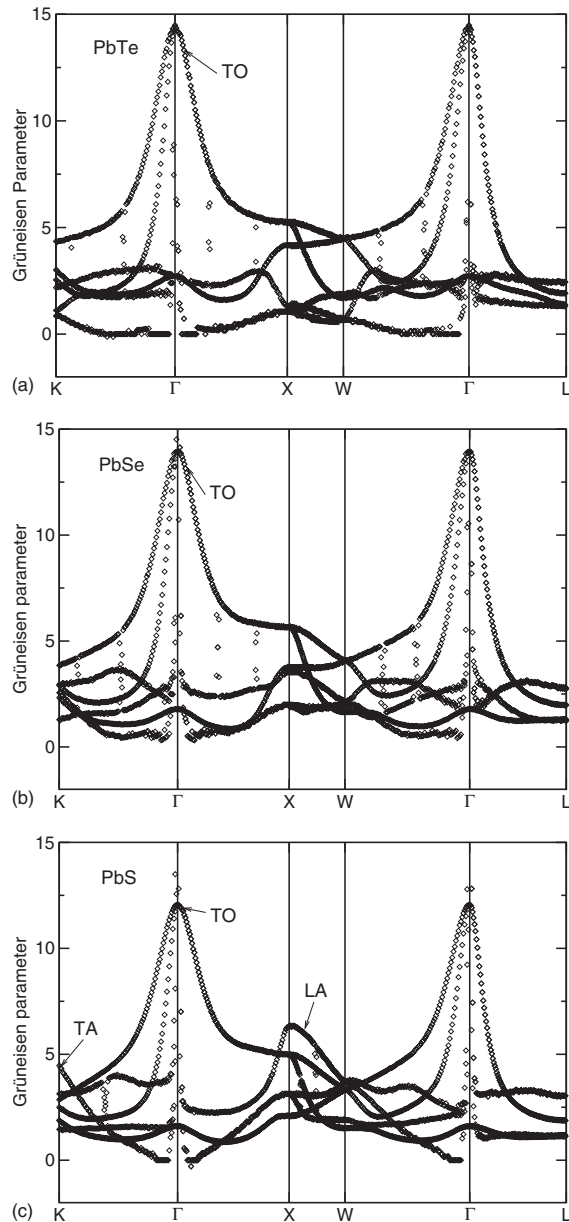
FIG. 9. Calculated Grüneisen parameter with respect to the wave vector for (a) PbTe, (b) PbSe, and (c) PbS, respectively. The top branches including the peaks at Γ points belong to the TO vibrational modes. For PbS, the Grüneisen parameters of LA and TA branches are found to be very large in the regions of $X \to W$ and $\Gamma \to K$, respectively.

The phonon dispersion and phonon DOS are calculated using the direct force-constant method. Our calculations show a large LO/TO splitting at Γ point caused by the very large Born effective charges, indicating that the lead chalcogenides are strong polar solids. The TO modes are very soft at Γ point, in agreement with previous studies. We also calculated the phonon frequencies when the unit cell is compressed or expanded and find that the TO and TA modes are very sensitive to the volume changes. The QHA is used to study the thermodynamic functions. The calculated free energy, vibrational entropy, internal energy, and heat capacity are in good agreement with the experimental data. Finally, the thermal transport properties are evaluated in terms of the Grüneisen parameters. The large acoustic-phonon mode Grüneisen parameters γ and the anharmonic effects of different phonon modes are further discussed by calculating the mode Grüneisen parameters. The calculated mode Grüneisen parameter peaks of the TO phonon modes are unusually large at Γ point. The very large LA and TA mode Grüneisen parameters are responsible for the highest γ of PbS.

As a remark on the GGA method used in our studies, it is found that the underestimation on electronic band gaps and the overestimation on lattice constants by GGA may cause deviations in calculating dielectric constant and thermal conductivity. However, accurate predictions of the phonon properties and thermodynamic functions are achieved using GGA.

ACKNOWLEDGMENTS

[1] R. Dalven, *Solid State Physics* (Academic, New York, 1973), Vol. 18.

[2] B. A. Efimave, L. A. Kolomoets, Yu. I. Ravich, and T. S. Stavitskaya, Sov. Phys. Semicond. **4**, 1653 (1971).

[3] H. J. Goldsmid, *Thermoelectric Refrigeration* (Plenum, New York, 1964).

[4] R. Venkatasubramanian, E. Siivola, T. Colpitts, and B. O'Quinn, Nature (London) **413**, 597 (2001).

[5] L. D. Hicks and M. S. Dresselhaus, Phys. Rev. B **47**, 12727 (1993).

[6] M. S. Dresselhaus, G. Chen, M. Y. Tang, R. Yang, H. Lee, D. Wang, Z. Ren, J. P. Fleurial, and P. Gogna, Adv. Mater. (Weinheim, Ger.) **19**, 1043 (2007).

[7] B. C. Sales, D. Mandrus, and R. K. Williams, Science **272**, 1325 (1996).

[8] C. Uher, in *Semiconductors and Semimetals*, edited by T. M.

Tritt (Academic, New York, 2000), Vol. 69, p. 139.

[9] G. S. Nolas, G. A. Slack, and S. B. Schujman, Semicond. Semimetals **69**, 255 (2001).

[10] T. C. Harman, P. J. Taylor, M. P. Walsh, and B. E. LaForge, Science **297**, 2229 (2002).

[11] H. Beyer, J. Nurnus, H. Bottner, A. Lambrecht, T. Roch, and G. Bauer, Appl. Phys. Lett. **80**, 1216 (2002).

[12] K. F. Hsu, S. Loo, F. Guo, W. Chen, J. S. Dyck, C. Uher, T. Hogan, E. K. Polychroniadis, and M. G. Kanatzidis, Science **303**, 818 (2004).

[13] P. Poudeu, J. D'Angelo, H. Kong, A. Downey, J. L. Short, R. Pcionek, T. P. Hogan, C. Uher, and M. G. Kanatzidis, J. Am. Chem. Soc. **128**, 14347 (2006).

[14] J. Androulakis, C. Lin, H. Kong, C. Uher, C. Wu, T. Hogan, B. A. Cook, T. Caillat, K. M. Paraskevopoulos, and M. G. Kanatzidis, J. Am. Chem. Soc. **129**, 9780 (2007).

[15] J. P. Heremans, V. Jovovic, E. S. Toberer, A. Saramat, K. Kurosaki, A. Charoenphakdee, S. Yamanaka, and G. J. Snyder, Science **321**, 554 (2008).

[16] G. Martinez, M. Schluter, and M. L. Cohen, Phys. Rev. B **11**, 651 (1975).

[17] K. M. Rabe and J. D. Joannopoulos, Phys. Rev. B **32**, 2302 (1985).

[18] S. H. Wei and A. Zunger, Phys. Rev. B **55**, 13605 (1997).

[19] E. A. Albanesi, C. M. I. Okoye, C. O. Rodriguez, E. L. Peltzer y Blanca, and A. G. Petukhov, Phys. Rev. B **61**, 16589 (2000).

[20] M. Lach-hab, D. A. Papaconstantipoulos, and M. J. Mehl, J. Phys. Chem. Solids **63**, 833 (2002).

[21] K. Hummer, A. Grüneis, and G. Kresse, Phys. Rev. B **75**, 195211 (2007).

[22] J. An, A. Subedi, and D. J. Singh, Solid State Commun. **148**, 417 (2008).

[23] A. H. Romero, M. Cardona, R. K. Kremer, R. Lauck, G. Siegle, J. Serrano, and X. C. Gonze, Phys. Rev. B **78**, 224302 (2008).

[24] M. Cardona, R. K. Kremer, R. Lauck, G. Siegle, J. Serrano, and A. H. Romero, Phys. Rev. B **76**, 075211 (2007).

[25] D. M. Ceperley and B. J. Alder, Phys. Rev. Lett. **45**, 566 (1980).

[26] J. P. Perdew and A. Zunger, Phys. Rev. B **23**, 5048 (1981).

[27] J. P. Perdew, K. Burke, and M. Ernzerhof, Phys. Rev. Lett. **77**, 3865 (1996).

[28] G. Kresse and J. Furthmüller, Phys. Rev. B **54**, 11169 (1996).

[29] G. Kresse and D. Joubert, Phys. Rev. B **59**, 1758 (1999).

[30] H. J. Monkhorst and J. D. Pack, Phys. Rev. B **13**, 5188 (1976).

[31] K. Parlinski, Z. Q. Li, and Y. Kawazoe, Phys. Rev. Lett. **78**, 4063 (1997).

[32] K. Kunc and R. M. Martin, Phys. Rev. Lett. **48**, 406 (1982).

[33] R. D. King-Smith and D. Vanderbilt, Phys. Rev. B **47**, 1651 (1993).

[34] http://www.freeware.vasp.de

[35] R. Dalven, Infrared Phys. **9**, 141 (1969).

[36] A. J. Miller, G. A. Saunders, and Y. K. Yoḡurtcu, J. Phys. C **14**, 1569 (1981).

[37] *Numerical Data and Functional Relationships in Science and Technology*, Landolt-Bornstein, New Series, Vol. 17, edited by O. Madelung, M. Schulz, and H. Weiss (Springer, Berlin, 1983).

[38] N. M. Ravindra and V. K. Srivastava, Phys. Status Solidi A **58**, 311 (1980).

[39] L. E. Diaz-Sanchez, A. H. Romero, M. Cardona, R. K. Kremer, and X. Gonze, Phys. Rev. Lett. **99**, 165504 (2007).

[40] J. Serrano, R. K. Kremer, M. Cardona, G. Siegle, L. E. Diaz-Sanchez, and A. H. Romero, Phys. Rev. B **77**, 054303 (2008).

[41] W. Cochran, R. A. Cowley, G. Dolling, and M. M. Elcombe, Proc. R. Soc. London, Ser. A **293**, 433 (1966).

[42] M. M. Elcombe, Proc. R. Soc. London, Ser. A **300**, 210 (1967).

[43] G. Raunio, L. Almqvist, and R. Stedman, Phys. Rev. **178**, 1496 (1969).

[44] S. Klotz, Z. Kristallogr. **216**, 420 (2001).

[45] G. Rousse, S. Klotz, A. M. Saitta, J. Rodriguez-Carvajal, M. I. McMahon, B. Couzinet, and M. Mezouar, Phys. Rev. B **71**, 224116 (2005).

[46] R. Ahuja, Phys. Status Solidi A **235**, 341 (2003).

[47] S. Baroni, S. de Gironcoli, and A. D. Corso, Rev. Mod. Phys. **73**, 515 (2001).

[48] D. H. Parkinson and J. E. Quarrington, Proc. Phys. Soc., London, Sect. A **67**, 569 (1954).

[49] D. T. Morelli and J. P. Heremans, Appl. Phys. Lett. **81**, 5126 (2002).

[50] A. A. El-Sharkawy, A. M. A. El-Azm, M. I. Kenawy, A. S. Hillal, and H. M. Abu-Basha, Int. J. Thermophys. **4**, 261 (1983).

[51] H. Olijnyk, A. P. Jephcoat, D. L. Novikov, and N. E. Christensen, Phys. Rev. B **62**, 5508 (2000).

[52] Z. Li and J. S. Tse, Phys. Rev. B **61**, 14531 (2000).

[53] P. Piekarz, P. T. Jochym, K. Parlinski, and J. Lazewski, J. Chem. Phys. **117**, 3340 (2002).